Molecular and Electronic Structure of [$Mn^{V}N$(cyclam−acetato)]PF_6. A Combined Experimental and DFT Study

Craig A. Grapperhaus,[†,‡] Eckhard Bill,[†] Thomas Weyhermüller,[†] Frank Neese,*[,§] and Karl Wieghardt*[,†]

Max-Planck-Institut für Strahlenchemie, Stiftstrasse 34−36, D-45470 Mülheim an der Ruhr, Germany, and Fakultät für Biologie, Universität Konstanz, D-78457 Konstanz, Germany

Received December 6, 2000

From the reaction of Li(cyclam−acetate), $MnCl_2 \cdot 4H_2O$, and KPF_6 in methanol brown microcrystals of [Mn^{III}-Cl(cyclam−acetato)]PF_6 (**1**) were obtained in the presence of air (cyclam−acetic acid = 1,4,8,11-tetraazacyclotetradecane-1-acetic acid). The reaction of **1** in aqueous NH_3 solution with NaOCl produced blue crystals of [$Mn^{V}N$(cyclam−acetato)]PF_6 (**2**). Complexes **1** and **2** were characterized by single-crystal X-ray crystallography, IR and Raman, electronic absorption, and ^{1}H, ^{13}C, and ^{15}N NMR spectroscopies. Their magnetochemistry as well as their electrochemistry have been investigated. The complexes [MnN(cyclam−acetato)]$^{+/2+}$ were studied by theoretical calculations at the DFT and semiempirical levels in order to obtain more insight into the ground and excited states of the $Mn^{V}\equiv N$ unit. Structural and spectroscopic parameters were successfully calculated and compared to experiment. A pictorial description of the bonding has been developed.

Introduction

Recently we reported the synthesis of a series of nitrido complexes of chromium(V),[1] manganese(V),[2] and even iron(V)[3] complexes containing spectroscopically innocent, saturated amines derived from the macrocycle 1,4,8,11-tetraazacyclotetradecane (cyclam) and its pendent arm derivative 1,4,8,11-tetraazacyclotetradecane-1-acetate (cyclam−acetate).[4] These octahedral complexes are ideally suited for studying the electronic structure of these d^n (n = 1, 2, and 3) configurated M≡N systems in depth because their electronic spectra are unperturbed by ligand and ligand-to-metal based absorption bands.

In addition, we have also investigated the corresponding nitridocyanometalates of chromium(V) and manganese(V).[5−7] The complexes $[M(N)(CN)_5]^{3-}$ and *trans*-$[M(N)(CN)_4(py)]^{2-}$ (M = Cr, Mn) were also investigated by density functional theory (DFT) methods.[7] In general, good reproduction of the molecular structures, vibrational, and UV−vis spectra was obtained.

In a very recent report we have spectroscopically characterized the very reactive, octahedral species [$Fe^{V}N$(cyclam−acetato)]$^{+}$ in frozen solution at cryogenic temperatures.[4] We have not been able to isolate and structurally characterize a (nitrido)iron(V) species to date. Therefore, we felt that theoretical calculations using DFT methods might provide more insight into the bonding of such a species. Before embarking on this undertaking, we felt that it is necessary to calibrate the DFT methodology against an experimentally well-characterized, stable system.

We report here the synthesis, the molecular and electronic structure of [$Mn^{V}N$(cyclam−acetato)]PF_6 (**2**), and theoretical calculations at the DFT and semiempirical levels in order to obtain more insight into the ground and excited states of the $Mn^{V}\equiv N$ unit.

In recent years density functional theory has become an increasingly useful tool to complement experimental studies. The success of DFT is mainly due to the fact that it describes transition metal ion containing systems more reliably than Hartree−Fock theory. It is also computationally more economic than wave function based methods with inclusion of electron correlation (see ref 8 for a recent review). Although under theoretical dispute, the orbitals delivered by DFT allow a single-particle type interpretation of chemical bonding and, thereby, lead to pictorial insight into the chemical and spectroscopic properties of the compounds under investigation.[8b]

Experimental Section

Syntheses. The ligand 1,4,8,11-tetraazacyclotetradecane-1-acetic acid tetrahydrochloride and the corresponding lithium salt were synthesized via published methods.[4,9] The purity of the crude lithium salt as determined by elemental analysis is 48% by mass, as reported previously.[4]

[†] Max-Planck-Institut für Strahlenchemie.
[‡] Current address: Department of Chemistry, University of Louisville, Louisville, KY 40292.
[§] Universität Konstanz.

(1) Meyer, K.; Bendix, J.; Bill, E.; Weyhermüller, T.; Wieghardt, K. *Inorg. Chem.* **1998**, *37*, 5180.
(2) Meyer, K.; Bendix, J.; Metzler-Nolte, N.; Weyhermüller, T.; Wieghardt, K. *J. Am. Chem. Soc.* **1998**, *120*, 7260.
(3) Meyer, K.; Bill, E.; Mienert, B.; Weyhermüller, T.; Wieghardt, K. *J. Am. Chem. Soc.* **1999**, *121*, 4859.
(4) Grapperhaus, C. A.; Mienert B.; Bill, E.; Weyhermüller, T.; Wieghardt, K. *Inorg. Chem.* **2000**, *39*, 5306.
(5) Bendix, J.; Meyer, K.; Weyhermüller, T.; Bill, E.; Metzler-Nolte, N.; Wieghardt, K. *Inorg. Chem.* **1998**, *37*, 1767.
(6) Bendix, J.; Weyhermüller, T.; Bill, E.; Wieghardt, K. *Angew. Chem., Int. Ed. Engl.* **1999**, *38*, 2766.
(7) Bendix, J.; Deeth, R. J.; Weyhermüller, T.; Bill, E.; Wieghardt, K. *Inorg. Chem.* **2000**, *39*, 930.
(8) (a) Koch, W.; Holthausen, M. C. A. *A Chemist's Guide to Density Functional Theory*; Wiley-VCH: Weinheim, New York, Chichester, Brisbane, Singapore, Toronto, 2000. (b) Bickelhaupt, F. M.; Baerends, E. J. In *Reviews in Computational Chemistry*; Lipkowitz, K. B., Boyd, D. B., Eds.; VCH Publishers: New York, 2000; Vol. 15, pp 1ff.
(9) Struder, M.; Kaden, T. A. *Helv. Chim. Acta* **1986**, *69*, 2081.

10.1021/ic001370r CCC: $20.00
Published on Web 07/07/2001

[Mn^{III}Cl(cyclam−acetato)]PF$_6$ (1). To 6.92 g (3.32 g; 12.9 mmol) of crude Li(cyclam−acetate) dissolved in 50 mL of degassed methanol was added via addition funnel 3.03 g (15.6 mmol) of $MnCl_2 \cdot 4H_2O$ in 50 mL of degassed methanol. After 8 h reflux, the colorless reaction mixture was exposed to air. To the darkened solution was added a slurry of 3.00 g (16.3 mmol) of KPF_6 in 10 mL of H_2O. After stirring overnight in air, the crude product was collected by filtration. From the brown precipitate, **1** was extracted in 6 × 100 mL hot acetonitrile yielding a pure, yellow powder upon evaporation of the solvent. Yield: 2.43 g, 43%. Crystals suitable for X-ray analysis were obtained by ether diffusion into a concentrated acetonitrile solution of **1**. IR (KBr; $\nu_{selected}$ (cm^{-1})): 3245 (N−H), 1638 (C═O), 1301, 1088, 1048, 1035, 840, 558 (PF_6). ESI mass spec: m/z = 347 (347 expected for [Mn^{III}Cl(cyclam−acetato)]$^+$. Anal. Calcd for $C_{12}H_{25}N_4O_2MnClPF_6$: C, 29.25; H, 5.11; N, 11.37. Found: C, 29.16; H 5.18; N, 11.44.

[Mn^{V}N(cyclam−acetato)]PF$_6$ (2). To 0.50 g (1.01 mmol) of **1** in 50 mL of H_2O was added 1.0 mL of aqueous ammonia (25%) dropwise. To the resulting orange solution was added dropwise 1.0 mL of aqueous NaOCl (13% active chlorine) yielding a brown reaction mixture. After 15 min stirring, solid MnO_2 was removed by filtration. The clear, green filtrate was allowed to slowly evaporate to yield deep blue crystals of **2** within 2−3 days which were washed with a minimum of cold water and dried under vacuum. Yield: 75 mg, 16%. IR (KBr; $\nu_{selected}$ (cm^{-1})): 3313, 3276 (N−H), 2943−2890, 1631 (C═O), 1099, 1023, 840, 559 (PF_6). Raman ($\nu_{selected}$ (cm^{-1}): 1011 (Mn≡N). ESI mass spec: m/z = 326 (326 expected for [Mn^{V}N(cyclam−acetato)]$^+$. UV/vis recorded in water (λ_{max}, nm (ϵ, M^{-1} cm^{-1})): 212 (450), 265 (200), 510 (20), 590 (15), 850 (1). Anal. Calcd for $C_{12}H_{25}N_5O_2MnPF_6$: C, 30.58; H, 5.35; N, 14.86. Found: C, 30.26; H 5.38; N, 14.93.

Physical Measurements. Infrared spectra (400−4000 cm^{-1}) as KBr disks or as acetonitrile solutions and Raman spectra (100−3600 cm^{-1}) as powder samples were recorded on a Perkin-Elmer 2000 FT-IR/FT-NIR spectrometer with a resolution of 4 cm^{-1}. For the Raman spectra a diode pumped Nd:YAG laser (λ = 1064 nm) was used. UV−visible measurements were made with a Perkin-Elmer Lambda 19 spectrophotometer in the range of 200−1600 nm. Cyclic voltammograms were recorded as acetonitrile solutions with 0.1 M tetra-*n*-butylammonium hexafluorophosphate (TBAHFP) as supporting electrolyte using an EG & G potentiostat/galvanostat (model 273A) and are referenced versus ferrocenium/ferrocene. Elemental analysis were performed by H. Kolbe Mikroanalysis in Mülheim an der Ruhr, Germany. ^{1}H and ^{13}C NMR measurements were recorded in deuterated solvents on a 400 MHz Bruker AMX series spectrometer. Electrospray ionization mass spectra were determined using a Finnigan MAT 95 spectrometer, Finnigan GmbH, Bremen. Temperature-dependent magnetic susceptibilities on solid samples were measured on a SQUID magnetometer (Quantum Design) at 1.0 T unless otherwise noted (2.0−300 K) with diamagnetic corrections made using tabulated Pascal constants.[10]

X-ray Crystallography. A yellow crystal of **1** and a blue crystal of **2** were each mounted in sealed glass capillaries. Graphite monochromated Mo Kα radiation (λ = 0.710 73 Å) was used. Crystallographic data are listed in Table 1. Intensity data for each of the compounds were collected at 100(2) K on a Siemens SMART CCD-detector system equipped with a cryogenic nitrogen cold stream. The data were corrected for Lorentz and polarization effects. A semiempirical absorption correction was made using the SADABS program.[11] The solution, refinements, and graphical representation of the structure were performed using the Siemens ShelXTL software package.[12] The structure was solved and refined by direct methods and difference Fourier techniques. Neutral atom scattering factors were used. All hydrogen atoms were placed at calculated positions and refined as riding atoms with isotropic displacement parameters. All non-hydrogen atoms were refined anisotropically except the minor part of a disordered acetonitrile molecule in **1**. A split atom model was used here. The major component with an occupation factor of 0.75 was anisotropically refined, while the minor part with a given occupation factor of 0.25 was isotropically refined. The PF_6^- anion in **1** is disordered by a 45° rotation along the C4 axis of the anion. Occupancies of 0.5 were used, and both parts were anisotropically refined.

Table 1. Crystallographic Data for **1**·MeCN and **2**

	1·MeCN	**2**
empirical formula	$C_{14}H_{28}ClF_6MnN_5O_2P$	$C_{12}H_{25}F_6MnN_5O_2P$
fw	533.77	471.28
space group	$P\bar{1}$	$P2_1/c$
a, Å	7.965(1)	8.684(1)
b, Å	12.382(2)	11.902(2)
c, Å	12.529(2)	18.154(2)
α, deg	114.20(2)	90
β, deg	98.28(2)	98.74(3)
γ, deg	94.28(2)	90
V, Å	1103.0(3)	1854.6(4)
Z	2	4
T, K	100	100
radiation λ, Å	0.710 73	0.710 73
ρ_{calcd}, g cm^{-3}	1.607	1.688
μ(Mo Kα), cm^{-1}	8.63	8.75
reflns collected	8206	18 830
unique reflns/obs [$I > 2\sigma(I)$]	3736/2784	6412/5222
no. of params	320	244
R1[a] [$I > 2s$**(I)**]	0.0583	0.0350
wR2[b] [$I > 2s$**(I)**]	0.1511	0.0878

[a] $R1 = \sum||F_o| - |F_c||/\sum|F_o|$, $R_W = [\sum w(|F_o| - |F_c|)^2/\sum wF_o^2]^{1/2}$, where $w = 4F_o^2/\sigma^2(F_o^2)$. [b] $wR2 = [\sum[w(F_o^2 - F_c^2)^2]/\sum[w(F_o^2)]^2]^{1/2}$, where $w = 1/\sigma^2(F_o^2) + (aP)^2 + bP$, $P = (F_o^2 + 2F_c^2)/3$.

DFT and Semiempirical Calculations. All coordinates were optimized by unconstrained geometry optimization at the RI-BP86 level using the TurboMole 5.2 program system.[13] BP86 specifies the local density approximation (VWN-5 functional[14]) together with the gradient corrected exchange functional of Becke[15] for exchange and the gradient corrected functional of Perdew[16] for correlation. The computationally efficient SV(P) basis of Schäfer et al.[17] was used (this basis is of split valence plus polarization quality: i.e., Cu, 14s9p5d contracted as {63311/531/41}; C,N,O, 7s4p1d contracted as {511/31/1}; H, 4s contracted as {31}) together with the so-called resolution of the identity (RI) approximation for the Coulomb repulsion energy.[18] The auxiliary basis sets were reported by Eichkorn et al.[19] The calculations employed grid 1 for the SCF iterations and grid 3 for the final energy and gradient evaluation.[20] The geometry search was carried out in "generalized natural internal coordinates" recently described by von Arnim and Ahlrichs.[21] The convergence criteria were 10^{-6} Eh for the total energy and 10^{-3} Eh/bohr for the internal gradient norm. All calculations were of the spin unrestricted type with $M_S = 0$ for the Mn(V) nitrido complex and $M_S = {}^1/_2$ for the Mn(VI) nitrido complex. The spin unrestricted Mn(V) calculation converged to a closed shell state. Starting geometries came from molecular mechanics calculations with the MM3 parametrization as implemented in the CAChe program.[22]

(10) *Theory and Application of Molecular Diamagnetism*; Mulay, L. N.; Boudreaux, E. A., Eds.; Wiley-Interscience: New York, 1976.
(11) Sheldrick, G. M. Universität Göttingen, 1994.
(12) *ShelXTL*, Version 5; Siemens Analytical X-ray Instruments, Inc.: 1994.
(13) Ahlrichs, R.; Bär, M.; Baron, H. P.; Bauernschmitt, R.; Böcker, S.; Ehrig, M.; Eichkorn, K.; Elliott, S.; Furche, F.; Haase, F.; Häser, M.; Horn, H.; Huber, C.; Huniar, U.; Kattanek, M.; Kölmel, C.; Kollwitz, M.; May, K.; Ochsenfeld, C.; Öhm, H.; Schäfer, A.; Schneider, U.; Treutler, O.; von Arnim, M.; Weigend, F.; Weis, P.; Weiss, H. *TurboMole−Program System for ab initio Electronic Structure Calculations*, Version 5.2; Universität Karlsruhe: Karlsruhe, Germany, 2000.
(14) Vosko, S. H.; Wilk, L.; Nusair, M. *Can. J. Phys.* **1980**, *58*, 1200.
(15) Becke, A. D. *J. Chem. Phys.* **1986**, *84*, 4524.
(16) Perdew, J. P. *Phys, Rev. B* **1986**, *33*, 8822.
(17) Schäfer, A.; Horn, H.; Ahlrichs, R. *J. Chem. Phys.* **1992**, *97*, 2571.
(18) (a) Baerends, E. J.; Ellis, D. E.; Ros, R. *Chem. Phys.* **1973**, *2*, 41. (b) Dunlap, B. I.; Connolly, J. W. D.; Sabin, J. R. *J. Chem. Phys.* **1979**, *78*, 3369. (c) Vahtras, O.; Almlöf, J. E.; Feyereisen, M. W. *Chem. Phys. Lett.* **1993**, *213*, 514.
(19) (a) Eichkorn, K.; Treutler, O.; Öhm, H.; Häser, M.; Ahlrichs, R. *Chem. Phys. Lett.* **1995**, *242*, 652. (b) Eichkorn, K.; Weigend, F.; Treutler, O.; Ahlrichs, R. *Theor. Chem. Acc.* **1997**, *97*, 119.
(20) Treutler, O.; Ahlrichs, R. *J. Chem. Phys.* **1995**, *102*, 346.
(21) von Arnim, M.; Ahlrichs, R. *J. Chem. Phys.* **1999**, *111*, 9183.

Excited-state energies and oscillator strengths were computed within the time-dependent density functional framework (TD-DFT[23]) as implemented in the TurboMole program.[24] For these calculations the size of the molecule was reduced by deleting the carbon atoms of the cyclam ligand and saturating the ligating nitrogens with hydrogens. Care was taken to add the hydrogens in exactly the same orientation as the carbon atoms in the complete structure. In this way, the full steric constraints of the ligand framework are taken into account but the smaller size of the model allows more accurate basis sets to be used in the property calculations. For the TD-DFT calculation the TZVP basis set of Schäfer et al.[25] was chosen for all atoms (this basis is of triple-ζ plus polarization quality: i.e., Cu, 14s10p5d contracted as {62111111/331111/311}; C,N,O, 10s6p1d contracted as {511111/411/1}; H, 5s1p contracted as {311/1}).

For the orbital plots the BP86 calculations on the small model were repeated with the program ORCA.[26] The SV(P) basis was used to describe the ligand and the TZVP basis on the Mn and nitrido nitrogens. The RI approximation was not used. The results of this calculation were very similar to the full TZVP calculation in terms of orbital energies and bonding parameters. The surface plots were drawn through an interface of ORCA to the gOpenMol package.[27]

Semiempirical calculations employed the INDO/S method of Zerner and co-workers[28] and were also carried out with the program ORCA. Excited states were calculated by single excitation configuration interaction (CIS) from the restricted Hartree−Fock (RHF) reference wave function for the truncated model of the $[(cyclam-acetato)Mn^{V}N]^+$ complex within a 32 × 28 orbital window. CI calculations with single and double excitations from the RHF ground state (CISD) lead to an unbalanced description that more strongly stabilized the ground state relative to the excited states. A multireference CI (MR−Cl) calculation with single and double excitations relative to the ground and the "d−d" singly excited states was also carried out. This calculation treats the ground and excited states on an equal footing and is expected to lead to a more balanced overall description. The results of this calculation were similar to that of the CIS calculation.

Results and Discussion

Syntheses and Characterization. To provide a stable, crystalline analogue of the highly reactive $[Fe^{V}N(cyclam-acetato)]^+$, the corresponding manganese derivative and its chloride precursor complex were synthesized. The synthetic protocol and labeling scheme are outlined in Scheme 1. Li(cyclam−acetate) reacts with $Mn(II)Cl_2 \cdot 4H_2O$ to yield, upon aerial oxidation and addition of KPF_6, $[MnCl(cyclam-acetato)]PF_6$ (**1**) as a crude brown solid. Pure **1** is obtained as a yellow solid from the crude material after repeated extractions with hot acetonitrile and evaporation of the solvent. The blue

Scheme 1

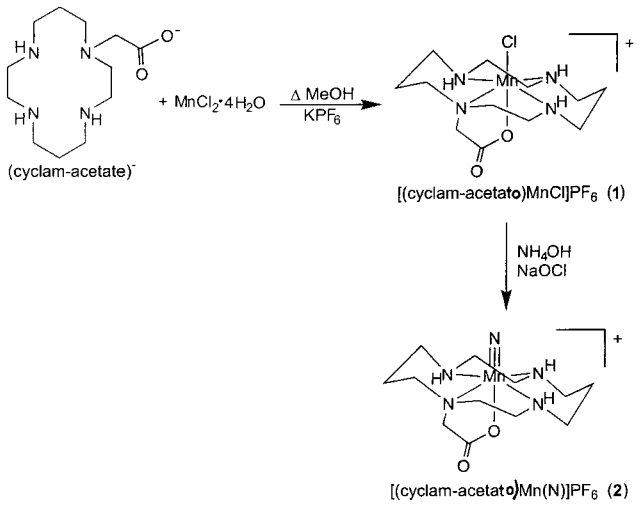

(nitrido)manganese(V) derivative, $[MnN(cyclam-acetato)]PF_6$ (**2**), is prepared via the NH_3/NaOCl method first described by Buchler.[29]

For previously reported hexadentate (nitrido)manganese(V) complexes, the $\nu(Mn{\equiv}^{14}N)$ stretching frequency varies from 983 to 1045 cm^{-1}, depending on the donor ability of the ligand trans to nitrido. Pentacoordinate Mn(V)≡N complexes typically display a $\nu(Mn{\equiv}^{14}N)$ of ∼1050 cm^{-1}.[30−33] The Raman spectrum of **2** displays a band at 1011 cm^{-1} attributable to $\nu(Mn{\equiv}^{14}N)$ which shifts by 23 cm^{-1} (27 cm^{-1} expected) to 988 cm^{-1} for the $Mn{\equiv}^{15}N$ derivative. Not unexpectedly, this value is similar to that observed for *trans*-$[MnCl(N)(cyclam)]^+$ (1006 cm^{-1})[2] consistent with coordination of the pendant acetate functionality trans to nitrido. Naturally, the acetate coordination is best evidenced in the infrared spectrum which shows a ν(CO) stretching frequency at 1631 cm^{-1} compared to 1730 cm^{-1} for H(cyclam−acetate).[9] For **1**, it is observed at 1638 cm^{-1}.

The magnetic susceptibility of **1** as a function of temperature could not be satisfactorily simulated assuming a manganese(III) monomer (d^4, $S = 2$). Data were collected over three external field strengths and fitted using the Heisenberg, Dirac, van Vleck model with the spin-Hamiltonian $H = -2JS_1 \cdot S_2$ ($S_1 = S_2 = 2$) and $g = 2.000$ (fixed). The data were successfully fitted assuming a small coupling constant ($J = -0.34$ cm^{-1}), a zero field splitting parameter $|D|$ of 3.38 cm^{-1} and a rhombicity parameter E/D of 0.136. As shown in Figure 1, the magnetic moment of **1** measured at 1 T varies from 6.94 μ_B at 260 K to 3.22 μ_B at 2 K and is consistent with the presence of weak dimers held together by hydrogen bonds (vida infra) of **1** in the solid state. Magnetic susceptibility measurements of **2** indicate a low-spin d^2 configuration as previously observed for other (nitrido)Mn(V) complexes.[2,30,31,33,34] The data were simulated with a significant TIP contribution of 140×10^{-6} cm^{-3} mol^{-1} and a small (0.4%) paramagnetic ($S = 2$) impurity.

(22) *Quantum CAChe*, Version 3.2; Oxford Molecular Ltd.: Oxford, U.K., 1999.
(23) (a) Runge, E.; Gross, E. K. U. *Phys. Rev. Lett.* **1984**, *52*, 997. (b) Gross, E. K. U.; Dobson, J. F.; Petersilka, M. In *Density Functional Theory*; Nalewajski, R. F., Ed.; Springer Series Topics in Current Chemistry Vol. 181; Springer: Berlin, Heidelberg, 1996; p 81.
(24) (a) Bauernschmitt, R.; Ahlrichs, R. *Chem. Phys. Lett.* **1996**, *256*, 454. (b) Bauernschmitt, R.; Häser, M.; Treutler, O.; Ahlrichs, R. *Chem. Phys. Lett.* **1997**, *264*, 573.
(25) Schäfer, A.; Huber, C.; Ahlrichs, R. *J. Chem. Phys.* **1994**, *100*, 5829.
(26) Neese, F. *ORCA−An ab Initio, DFT and Semiempirical Electronic Structure Package*, Version 2.0, Revision 87; Universität Konstanz: Konstanz, Germany, 2000.
(27) Laaksonen, L. *The gOpenMol effort*, Version 1.4; Espoo, Finland, 2000 (obtained from http://www.csc.fi/∼laaksone/gopenmol/gopenmol.html).
(28) (a) Ridley, J.; Zerner, M. C. *Theor. Chim. Acta* **1973**, *32*, 111. (b) Bacon, A. D.; Zerner, M. C. *Theor. Chim. Acta* **1979**, *53*, 21. (c) Zerner, M. C.; Loew, G. H.; Kirchner, R. F.; Mueller-Westerhoff, U. T. *J. Am. Chem. Soc.* **1980**, *102*, 589. (d) Anderson, W. P.; Edwards, W. D.; Zerner, M. C. *Inorg. Chem.* **1986**, *25*, 2728.
(29) (a) Buchler, J. W.; Dreher, C.; Lay, K.-L. *Z. Naturforsch., B: Anorg. Chem., Org. Chem.* **1982**, *37B*, 1155−1162.
(30) Du Bois, J.; Hong, J.; Carreira, E. M.; Day, M. W. *J. Am. Chem. Soc.* **1996**, *118*, 915−916.
(31) Hill, C. L.; Hollander, F. J. *J. Am. Chem. Soc.* **1982**, *104*, 7318−7319.
(32) Du Bois, J.; Tomooka, C. S.; Hong, J.; Carreira, E. M.; Day, M. W. *Angew. Chem.* **1997**, *109*, 1722−1724; *Angew. Chem., Int. Ed. Engl.* **1997**, *36*, 1645−1647.
(33) Buchler, J. W.; Dreher, C.; Lay, K.-L.; Lee, Y. J. A.; Scheidt, W. R. *Inorg. Chem.* **1983**, *22*, 888−891.
(34) Niemann, A.; Bossek, U.; Haselhorst, G.; Wiehardt, K.; Nuber, B. *Inorg. Chem.* **1996**, *35*, 906−915.

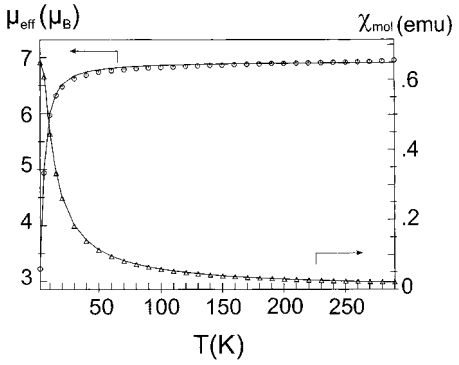

Figure 1. Temperature dependence of the magnetic moment (○), μ_{eff} (μ_B), and molar magnetic susceptibility (Δ), χ_{mol} (emu), of **1** (calculated per dimer). The solid line represents the best fit to the data (see text).

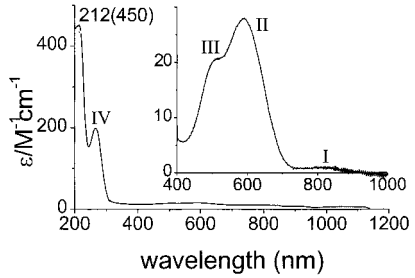

Figure 2. Electronic spectrum of **2** recorded in H_2O.

Based on the magnetic susceptibility results, it is not unexpected that the ^1H and ^{13}C NMR spectra of **2** (Figure S1 of the Supporting Information), recorded in D_2O, display chemical shifts and line widths typical of diamagnetic complexes. Due to conformational restraints enforced upon the cyclam by metal coordination and the reduction of symmetry resultant from the functionalization of one nitrogen, each carbon and hydrogen atom in **2** is magnetically inequivalent. Hence, the 12 carbon atoms of **2** are represented by 12 unique resonances in the ^{13}C NMR spectrum. The pair of resonances at 26.0 and 27.6 ppm are assigned to the apical carbons of the propylene linkers, while the resonance at 180 ppm clearly represents the carboxylate carbon. The other 9 resonances for the carbons adjacent to the amine donor atoms occur between 49.2 and 68.2 ppm and have not been specifically assigned. The integration of the ^1H spectrum is consistent with the solid-state structure (vida infra), and the ^{13}C NMR. The coupling is similar, albeit more complicated, to that observed in [Pt(cyclam)]-$(ClO_4)_2$ for which a full assignment has been made.[35]

The ^{15}N NMR spectrum was recorded in D_2O on a sample of **2** which had been enriched at the terminal nitrido with ^{15}N. The spectrum is dominated by a single resonance at 699 ppm versus nitromethane. Such extreme deshielding of the nitrogen nuclei has been previously observed with other (nitrido)-manganese(V) complexes.[2]

The electronic spectrum of **2** is shown in Figure 2 and is summarized in Table 2. Not unexpectedly, the spectrum of 2 is quite similar to that observed for the series *trans*-[Mn(N)(Y)-(cyclam)]$^+$ (see Table 2) and a similar band assignment can be made.[2] These assignments were corroborated for the previous series by calculations using the angular overlap model. Extending these results to the spectrum of **2**, the assignments of band I ($^1A_1 \rightarrow {}^3E$, $d_{xy} \rightarrow d_{xz}, d_{zy}$), band II ($^1A_1 \rightarrow {}^1E$, $d_{xy} \rightarrow d_{xz}, d_{zy}$), and band III ($^1A_1 \rightarrow {}^1A_2$, $d_{xy} \rightarrow d_{x2-y2}$) are attributed to the bands observed at 11 800, 16 700, and 19 900 cm^{-1}, respectively. The expected transition $^1A_1 \rightarrow {}^1B_1$ ($d_{xy} \rightarrow d_{z2}$) is tentatively assigned to the band at 37 700 cm^{-1} (265 nm). This is approximately 5500 to 7300 cm^{-1} higher in energy than that observed in the series *trans*-[(cyclam)Mn(N)(Y)]$^+$. However, for this series it was postulated that the ligand, Y, trans the nitrido is labile in solution and displaced by solvent, as evidenced by the similarity of the UV/vis spectra throughout the series. Displacement of the tethered acetate functionality by solvent is less likely. (In fact, there is a negative shift in the potential of the $Mn^{VI/V}$ redox couple with respect to the series *trans*-[(cyclam)Mn(N)(Y)]$^+$, and only a single peak is observed in the ESI-MS of **2,** which is attributed to [Mn(N)(cyclam−acetato)]$^+$.) Hence, the presence of a stronger σ donor in the position trans to nitrido in **2** will destabilize the d_{z^2} orbital, thus raising the energy of the transition, with respect to the earlier series of compounds.

The molecular structures of **1** and **2** have been determined by X-ray crystallography. Each of the cations is hexacoordinate, pseudooctrahedral with the four cyclam nitrogens occupying the equatorial positions and the carboxylate oxygen filling one of the axial sites. The sixth ligand, trans to the carboxylate, is chloride for **1** and nitride for **2**. A list of selected bond lengths and bond angles is provided in Table 3. In each of the complexes, the cyclam adopts the most favored trans III configuration as defined by Bosnich et al.[36]

Crystals of **1** contain a [MnCl(cyclam−acetato)]$^+$ cation, shown in Figure 3, two acetonitrile molecules, and a single uncoordinated hexafluorophosphate anion. As shown in the partial packing diagram, Figure S2 of the Supporting Information, each [MnCl(cyclam−acetato)]$^+$ cation is linked to two neighboring cations via a pair of interactions between Cl(1) and the hydrogen of N(2) (N(2)···Cl(1) = 3.22 Å) resulting in a Mn···Mn distance of 6.45 Å and a pair of H-bond linkages between N(4) and O(2) (N(4)···O(2) = 2.77 Å) resulting in a longer Mn···Mn distance of 7.27 Å. As expected for Mn(III) (d^4), **1** experiences a Jahn−Teller elongation along the Cl−Mn−O axis: Mn−O, 2.103(3) Å; Mn−Cl, 2.491(1) Å. The Mn−Cl bond is only slightly longer (∼0.028 Å) than the distance 2.463(2) Å observed in the dicationic [MnCl(cyclam−imidazole)]$^{2+}$.[37] The four cyclam nitrogens form a distorted plane with a mean deviation of 0.059 Å. The $Mn-N_{amine}$ distances of 2.034(3) and 2.026(3) Å for N(2) and N(4) are in the range observed for other manganese cyclam complexes.[2,37] The $Mn-N_{amine}$ distance to the tertiary amine N(1) is, as expected, slightly longer (2.079(4) Å) than the distance to N(3) of 2.070(4) Å which is trans to the N(1).

Crystals of **2** consist of [Mn(N)(cyclam−acetato)]$^+$ cations shown in Figure 4 and well-separated PF_6^- anions. The $Mn-N_{amine}$ distances of **2** are unchanged within experimental error from **1** even though the manganese has been formally oxidized by two electrons. The short $Mn-N_{nitrido}$ distance of 1.537(1) Å fits within the range observed for the series of [(cyclam)(Y)-Mn^VN] complexes previously reported.[2] The Mn−O bond of 2.126(1) for **2** (low-spin Mn(V)) is actually longer than that observed in the Jahn−Teller elongated **1** (high-spin Mn(III)) due to its position trans to the strongly π-donating nitrido ligand. In fact, and as observed with other (cyclam)(nitrido)Mn(V)-complexes, the Mn ion sits 0.212 Å above the distorted plane

(35) Chandrasekhar, S.; Waltz, W. L.; Prasad, L.; Quail, J. W. *Can. J. Chem.* **1997**, *75*, 1363−1374.

(36) (a) Bosnich, B.; Poon, C.-K.; Tobe, M. L. *Inorg. Chem.* **1962**, *4*, 1102−1108. (b) Adam, K. R.; Atkinson, I. M.; Lindoy, L. F. *Inorg. Chem.* **1997**, *36*, 480−481.

(37) Kimura, E.; Shionoya, M.; Yamauchi, T.; Shiro, M. *Chem. Lett.* **1991**, 1217−1220.

Table 2. Electronic Spectra of **2** and Related Complexes in Solution

		λ_{max}, nm (ϵ, M^{-1} cm^{-1})				
complex	solvent	I	II	III	IV	ref
2	H_2O	850(1)	590(15)	510(20)	265(200)	this work
trans-$[LMn(N)(CH_3CN)]^+$	CH_3CN	850(1)	581(34)	496(24)		2
	H_2O	844(1)	581(28)	495(19)	310(15)	
	$HClO_4$[a]	830(1)	570(27)	493(21)	329(12)	
trans-$[LMn(N)(ClO_4)]^+$	CH_3NO_2	820(1)	573(29)	497(23)	b	2
trans-$[LMn(N)(O_2CCF_3)]^+$	CH_3CN	850(1)	585(27)	~500(sh)	~360(sh)	2

[a] 9.2 M $HClO_4$ ($NaClO_4$). [b] Band not observed due to solvent absorption. L = cyclam.

Table 3. Selected Bond Lengths (Å) and Angles (deg) for **1** and **2**

1		**2**	
Mn−N1	2.079(4)	Mn−N1	2.061(1)
Mn−N2	2.034(2)	Mn−N2	2.032(1)
Mn−N3	2.070(4)	Mn−N3	2.036(1)
Mn−N4	2.026(3)	Mn−N4	2.047(1)
Mn−Cl	2.490(1)	Mn−N5	1.538(1)
Mn−O1	2.103(3)	Mn−O1	2.126(1)
C12−O1	1.275(6)	C12−O1	1.276(2)
C12−O2	1.238(5)	C12−O2	1.239(2)
N1−Mn−N2	87.2(2)	N1−Mn−N2	92.63(5)
N2−Mn−N3	94.7(2)	N2−Mn−N3	84.85(5)
N3−Mn−N4	85.1(2)	N3−Mn−N4	94.64(5)
N4−Mn−N1	93.0(2)	N4−Mn−N1	85.52(5)
N1−Mn−N3	172.6(1)	N1−Mn−N3	165.79(5)
N2−Mn−N4	179.3(1)	N2−Mn−N4	170.43(5)
O1−Mn−Cl	175.9(9)	O1−Mn−N5	176.44(5)

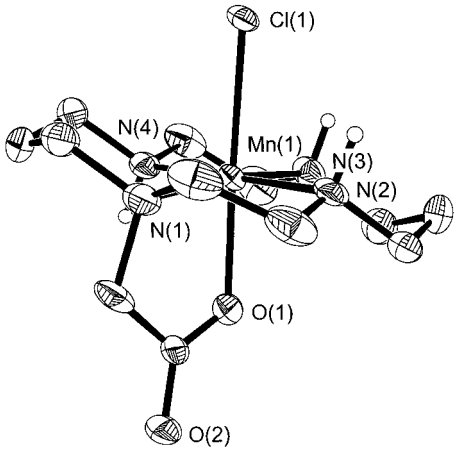

Figure 3. View of the molecular structure and atom labeling of the monocation in crystals of **1**. Small open circles represent amine hydrogen atoms. Other hydrogen atoms have been eliminated.

defined by the four cyclam nitrogens: mean deviation of 0.0413 Å, toward the nitrido ligand.

Electrochemical Investigations. The electrochemistry of **1** and **2** was investigated in acetonitrile solution with 0.1 M TBAHFP as supporting electrolyte. All potentials reported are referenced versus ferrocenium/ferrocene. A summary of observed electrochemical potentials is provided in Table 4.

Complex **2** displays a single oxidation and one reduction within the solvent window of acetonitrile. The oxidation is irreversible at slow scan rates (200 mV/s) but becomes reversible as the scan rate is increased (≥2.5 V/s). Thus, while the oxidation is electrochemically reversible, the oxidized species is unstable in solution; i.e., the process is chemically irreversible. Hence, cyclic voltammograms collected at low temperature (−30 °C) display reversible behavior at much lower scan rates, 400 mV/s. The oxidation, $E_{1/2}$ = +990 mV, is 270 mV more accessible than the $Mn^{VI/V}$ redox couple measured for [Mn(N)-(cyclam)$(NCCH_3)]^+$. The shift in redox potential is consistent with the exchange of the neutral solvent molecule with an anionic carboxylate donor.[2] The reduction of **2** requires very negative potentials, −2080 mV at 200 mV/s, and is irreversible even at fast scan rates. Complex **1** displays a reduction at −380 mV in acetonitrile assignable to a $Mn^{III/II}$ couple and a quasi-reversible oxidation at +650 mV.

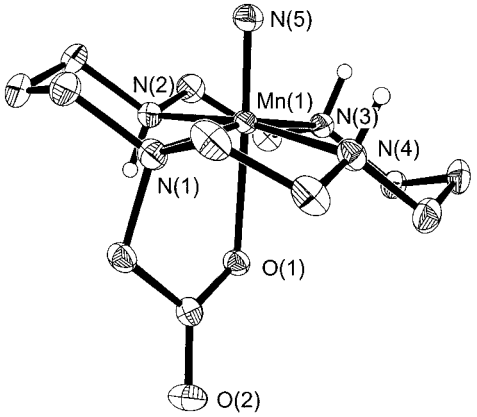

Figure 4. View of the molecular structure and atom labeling of the monocation in crystals of **2**. Small open circles represent amine hydrogen atoms. Other hydrogen atoms have been eliminated.

Table 4. Electrochemical Data[a] from Cyclic Voltammetry in Acetonitrile[b] of **1** and **2**

complex	$E_{1/2}$ (ΔE_p) (mV)	i_{pa}/i_{pc}	assignment
1	−380 (irr.)[c]		Mn(III)/Mn(II)
	+650 (120)	1.45	Mn(IV)/Mn(III)
2	−2080 (irr.)[c]		
	+ 990 (75)[d]	1.19[d]	Mn(VI)/Mn(V)

[a] All potentials are measured at a scan rate of 200 mV/s unless otherwise noted and are referenced to ferrocenium/ferrocene standard. [b] ~1 mM solution with 0.1 M TBAHFP supporting electrolyte measured versus $Ag/AgNO_3$ reference electrode. [c] The process is irreversible. The potential reported is the E_{pa} measured at 200 mV/s. [d] Measured at 400 mV/s and −30 °C.

Table 5. Geometrical Parameters Calculated for $[(cyclam-acetato)Mn^{V}N]^+$ (**2**) and $[(cyclam-acetato)Mn^{VI}N]^{2+}$ (**2′**) at the RI-BP86/SV(P) Level and Comparison to the Experimental Structure Parameters for **2**

complex	Mn≡N (Å)	Mn−N_{eq}[a] (Å)	Mn−OOC (Å)	θ[b] (deg)	N≡Mn−OOC (deg)
2 (calc)	1.528	2.086	2.053	96.3	176.3
2 (expt)	1.537	2.030	2.126	95.9	176.4
2 (calc)[c]	1.528	2.097	2.016	96.8	172.6

[a] Average of the four Mn−N_{cyclam} distances. [b] Average of the four N≡Mn−N_{cyclam} angles. [c] $[(cyclam-acetato)Mn^{VI}N]^{2+}$ (**2′**).

DFT Calculations. (a) Geometric Structure. The fully optimized structure of $[Mn^{V}N(cyclam-acetato)]^+$ (**2**) (Table 5) compares very well with the experimentally determined structure (Figure 4). The crucial Mn≡N bond length is almost exactly reproduced with an error of less than 0.01 Å. The other metal−ligand bond lengths show a larger deviation but are still

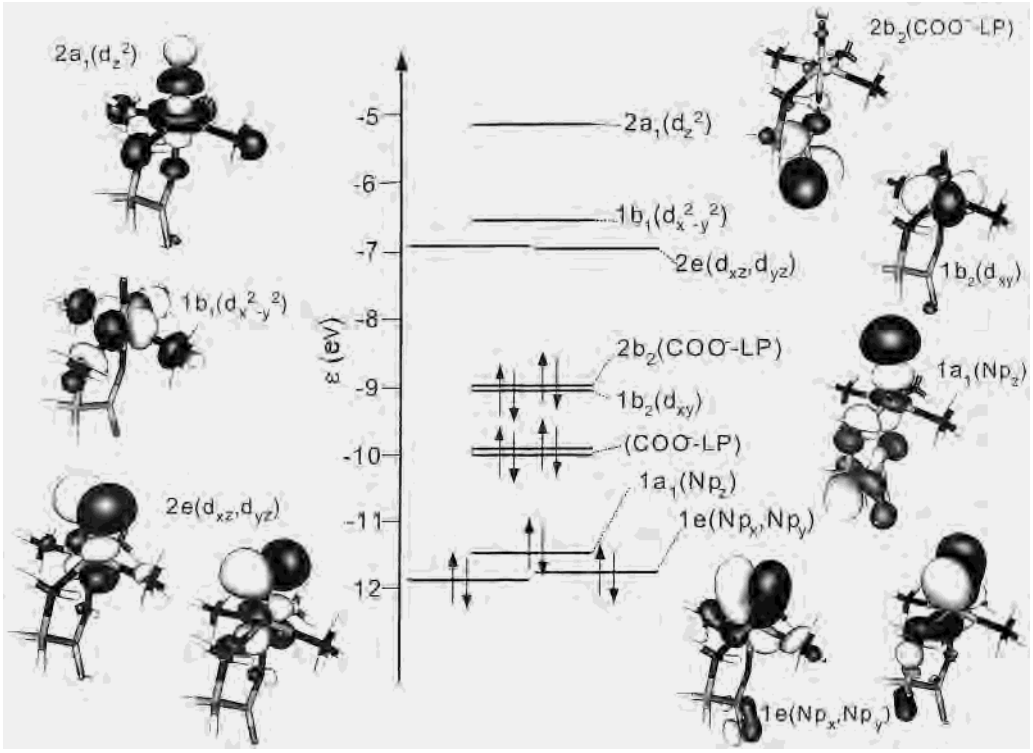

Figure 5. Molecular orbital energy level diagram for the ground state of **3** in the upper valence region derived from BP86 DFT calculations and surface plots of the MOs.

reasonable given the level of approximation and the complete neglect of crystal packing effects. The calculations also correctly predict that the manganese ion is located slightly above the plane spanned by the four cyclam nitrogens with an average N≡Mn−N_{cyclam} angle of 96.3° and the slight deviation of the N≡Mn−−OO*C* axis from 180°.

The structure of the one electron oxidized species, [Mn^{VI}N-(cyclam−acetato)]$^{2+}$ (**2′**) is very similar; there are only minimal changes in the structure upon one-electron oxidation of **2**. The Mn≡N distance does not change at all, while the other metal−ligand bonds show only small changes. This is consistent with a metal centered oxidation where the electron was removed from a predominantly nonbonding orbital, in agreement with the conclusions reached earlier for a closely related complex.[7]

The results demonstrate the utility of DFT methods in predicting the structures of large metal complexes well, even with the rather moderate basis sets used in this study. This is an important finding because it implies that the calculations can be used with some confidence to predict the structures of short-lived intermediates where an experimental structure determination is not possible and which are too large to be treated theoretically using more exhaustive basis sets. On the basis of the theoretical structures, the properties of possible intermediates can be predicted and compared to spectroscopic observations which will ultimately give insight into reaction mechanisms.

(b) Electronic Structure. The ligand field around the manganese ion in **2** is a distorted octahedron. For a d^2 system in octahedral symmetry the manganese d-orbitals are split into a t_{2g} and an e_g set, and from ligand field theory a triplet ground state must arise. However, **2** clearly has a singlet ground state. This behavior is typical of high valent metal ions with highly negatively charged donor ligands. The underlying reason is that the high effective nuclear charge on the metal strongly stabilizes the metal orbitals and brings them energetically close to the ligand orbitals. First, very strong mixing between the metal and ligand orbitals can occur (i.e. highly covalent bonds are formed between the metal and the ligand) which obscures a ligand field picture. Second, the highly negatively charged donor ligands, in the present case the nitrido nitrogen, have high-lying filled orbitals that are capable of forming σ and π bonds with the metal. Consequently, the high covalency is also very anisotropic, which leads to large orbital splittings within both the t_{2g} and e_g sets.

Table 6. Composition of Energies for the High-Lying Occupied and Unoccupied Valence Orbitals of [$(NH_3)_3(H_2NCH_2COO)Mn^{V}N]^+$ (**3**)[a]

orbital	occ.[b]	energy (eV)	% Mn	% $N_{nitrido}$	% COO	% rest
$1e_y$ (Np_y)	2	−11.943	42.2	37.9	6.9	13.0
$1e_x$ (Np_x)	2	−11.894	41.2	37.3	9.5	11.9
$1a_1$ (Np_z)	2	−11.640	18.1[c]	43.5	28.2	10.1
$1b_2$ (d_{xy})	2	−9.845	92.8	0.1	2.9	4.3
$2b_2$(COO⁻−LP)	2	−8.895	3.2	1.8	93.4	1.7
$2e_x$ (d_{xz})	0	−6.982	51.4	41.3	2.2	5.0
$2e_y$ (d_{yz})	0	−6.919	52.0	39.5	3.2	5.3
$1b_1$ ($d_{x^2-y^2}$)	0	−6.557	70.6	0.3	1.4	27.7
$2a_1$ (d_{z^2})	0	−5.141	33.2[d]	14.6	11.0	41.2
$3a_1$ (4s)	0	−4.706	33.9[d]	15.9	12.4	32.4

	MntN	Mn−N[e]	Mn−OOC
Wiberg bond order	3.21	0.65	0.52

[a] Results obtained with the BP86 functional together with the SV(P) basis set for the ligand and TZVP for the manganese and the nitrido ligand. Percentage contributions were obtained from a Löwdin population analysis. [b] Occupation number. [c] The Np_z/Mn-d_z^2 bonding character is distributed over several valence orbitals. [d] The Mn−d_z^2 is heavily mixed with the Mn-4s orbital next in energy. [e] Average of the four Mn−N_{amine} bond orders.

These are the basic effects observed in the orbital scheme of the abbreviated version of **2**, namely, [$(NH_3)_3(H_2NCH_2COO)$-$Mn^{V}N]^+$ (**3**) shown in Figure 5 and Table 6. As expected, the four lowest unoccupied orbitals are manganese based and antibonding between the metal and the ligands. Three of these orbitals ($2a_1$ (d_{z^2}), 1e (d_{xz},d_{yz})) have very large interactions with the nitrido ligand and are the antibonding counterparts of the

fully occupied orbitals $1a_1$ (Np_z) and 1e ($Np_{x,y}$) at lower energy. From the formal electron count this defines a genuine manganese−nitrogen triple bond which is consistent with the very short bond length observed experimentally at 1.537 Å and a Wiberg bond order of 3.21 calculated for this bond (Table 6). Since the mixing of metal and ligand orbitals in these MOs is so large, the bond has only a limited polarity consistent with the electroneutrality principle and earlier conclusions.[7] The fourth unoccupied metal based orbital is $1b_1$ ($d_{x^2-y^2}$), which is antibonding with the amine nitrogens. Finally, the fifth manganese based orbital is found as the second highest doubly occupied MO and corresponds to the manganese d_{xy} orbital which is essentially nonbonding (Figure 5). Thus, the formal electronic configuration at the manganese is $(d_{xy})^2$, as expected, but the actual situation is more complicated due to the large covalency of the Mn≡N bond that leads to large charge donation from the nitrido ligand to the manganese.

The domininant role of the nitrido ligand in the ligand field of **2** is also clearly observed in the orbital splitting patterns. The formally t_{2g} derived orbitals $1b_2$ (d_{xy}) and 2e (d_{xz},d_{yz}) are split by more than 2 eV. In fact, the very large π interaction brings the 2e (d_{xz},d_{yz}) close to the e_g derived orbital $1b_1$ ($d_{x^2-y^2}$), a situation first discussed for the VO^{2+} unit by Jørgensen[38] and Ballhausen and Gray.[39] Especially the latter authors have stressed the importance of highly covalent π-bonding for the understanding of the optical and magnetic properties of VO^{2+} containing complexes. This very large splitting is also the origin of the observed singlet ground state because the splitting easily exceeds the energy required to pair two electrons in the manganese d_{xy} orbital. The splitting within the e set is also large (>1.5 eV), again due to the strong σ-interaction of the nitrido ligand with the manganese that destabilizes the $2a_1$ (d_{z^2}) orbital.

In addition to these orbitals there are three orbitals in the upper valence region that can be identified with lone pairs of the COO^- group.

It is also evident from the Wiberg bond orders in Table 6 that the nitrido group exhibits a considerable trans effect. The bond orders for the $Mn-N_{amine}$ bonds are larger than for the Mn−OOC bond, although the anionic carboxylate ligand is commonly considered to be a stronger ligand than neutral aliphatic amines. This result is consistent with the observed bond lengths (Table 5), which show a rather long Mn−O bond (2.126 Å) compared to the average $Mn-N_{amine}$ bond length of 2.03 Å. That this trend in the bond lengths is not perfectly reproduced by the calculations is an indication that the strength of the trans effect in this system is somewhat underestimated by DFT. Interestingly, this is in sharp contrast to the previous observation that for nitridocyanometalates DFT strongly *overestimates* the trans effect.[7]

In conclusion, the ligand field of **2**, and by inference also other $Mn^{V}N$ complexes, is strongly dominated by the highly covalent Mn≡N triple bond that leads to a very short bond length, a high charge donation to the manganese, a considerable trans effect, and large splittings of orbitals that are formally degenerate in octahedral symmetry.

Excited-State Calculations. To get more insight into the excited states of the $Mn^{V}N$ unit, TD-DFT and INDO/S-CI calculations were carried out on the truncated models of **2**, namely $[(NH_3)_3(H_2NCH_2COO)MnN]^+$ (**3**) and (**4**). Two sets of calculations were carried out. One with the truncated model **3** and one with a truncated model where the metal−ligand bond lengths were adjusted to the experimental values in Table 5 (model **4**).

Table 7. Energies of the Singlet−Singlet and Singlet−Triplet Ligand Field Excited States for the Truncated $Mn^{V}N$ Models[a]

	TD-DFT (RIBP86)			INDO/S		
transition	**3**	**4**	**5**	**3**	**4**	**5**
$^1A_1 \rightarrow {}^1E$ ($d_{xy} \rightarrow d_{xz},d_{yz}$)	19 070	18 540	18 130	20 250	19 420	21 740
	19 320	19 120	18 780	20 610	19 830	22 180
$^1A_1 \rightarrow {}^1A_2$ ($d_{xy} \rightarrow d_{x^2-y^2}$)	19 800	22 140	22 740	12 160	14 950	15 670
$^1A_1 \rightarrow {}^1B_1$ ($d_{xy} \rightarrow d_{z^2}$)	31 520	31 680	33 620	28 100	38 650	30 170
$^1A_1 \rightarrow {}^3A_2$ ($d_{xy} \rightarrow d_{x^2-y^2}$)	11 720	14 810	15 420	7 480	10 470	11 225
$^1A_1 \rightarrow {}^3E$ ($d_{xy} \rightarrow d_{xz},d_{yz}$)	12 270	11 750	11 450	14 870	14 000	16 550
	12 740	12 260	12 030	15 280	14 470	17 070

[a] Transition energies are given in cm^{-1}. $[(NH_3)_3(H_2NCH_2COO)Mn^{V}N]^+$ (**3**); model **4** is the same as model **3** but with adjusted Mn-X bond lengths from Table 5; *trans*-$[(cyclam)(CH_3CN)MN^{V}N]^{2+}$ (**5**).

The results collected in Table 7 give conflicting interpretations on the experimental data. Both the INDO/S and the TD-DFT calculations predict the ^1E ($d_{xy} \rightarrow d_{xz},d_{yz}$) excited state around 19 000−20 000 cm^{-1}, very close to the band observed at 19 900 cm^{-1}. However, this band was assigned to the $^1A_2$ ($d_{xy} \rightarrow d_{x^2-y^2}$) transition (vide supra and ref 2). The $^1A_2$ ($d_{xy} \rightarrow d_{x^2-y^2}$) state is predicted to be at 14 950 cm^{-1} by INDO/S, in reasonable agreement with the band observed at 16 700 cm^{-1}, which was, however, assigned to the ^1E ($d_{xy} \rightarrow d_{xz},d_{yz}$) state. The TD-DFT calculation gives the $^1A_2$ ($d_{xy} \rightarrow d_{x^2-y^2}$) state at 22 140 cm^{-1}, i.e., *above* the ^1E ($d_{xy} \rightarrow d_{xz},d_{yz}$) state, in agreement with the earlier assignment.[2] However, the TD-DFT calculations also predict a series of low-lying, weak carboxylate to manganese LMCT transitions starting at ≈13 000 cm^{-1} for which there is no experimental evidence. The INDO/S calculations predict these states at energies above 30 000 cm^{-1}. All calculations corroborate the conclusion drawn above about the influence of the more strongly donating, anionic axial carboxylato ligand that significantly increases the energy of the $^1A_1 \rightarrow {}^1B_1$ ($d_{xy} \rightarrow d_{z^2}$) transition relative to a less strongly bound neutral ligand.

A similar result is obtained for the first two excited triplet states. The INDO/S calculations give the first excited triplet as the $^3A_2$ ($d_{xy} \rightarrow d_{x^2-y^2}$) state at 10 470 cm^{-1}, close to the experimentally observed weak band at 11 800 cm^{-1} and the ^3E ($d_{xy} \rightarrow d_{xz},d_{yz}$) state 3000−4000 cm^{-1} higher in energy. In the TD-DFT calculations based on the adjusted structure, **4**, the first excited triplet state is ^3E ($d_{xy} \rightarrow d_{xz},d_{yz}$), which is calculated to be very close to the experimental value, and the $^3A_2$ ($d_{xy} \rightarrow d_{x^2-y^2}$) state is predicted to be ≈2000 cm^{-1} higher in energy.

The differences in the spectral predictions between the INDO/S and the TD-DFT calculations point to differences in the σ versus π bond strength predicted by the two methods. While the π interactions seem to be fairly similar, based on the predictions for the ^{2S+1}E states, the σ-interaction with the amine ligands is predicted considerably weaker by the INDO/S method which leads to the prediction of the $^1A_2$ ($d_{xy} \rightarrow d_{x^2-y^2}$) state at lower energies than observed in the TD-DFT calculations.

To shed more light on this subject a second series of calculations was performed on a truncated model of the complex $[(cyclam)(H_3CCN)Mn^{V}N]^{2+}$ which had been studied in detail before.[2] This model is denoted **5**. The values calculated by the INDO/S method (Table 7) compare favorably with the experimental transition energies determined in ref 2. However, the same reversal of band assignments as that for **2** is obtained. The TD-DFT calculations give equally good numerical agreement with the experimentally observed band positions and the

(38) Jörgensen, C. K. *Acta Chem. Scand.* **1957**, *11*, 73.
(39) Ballhausen, C. J.; Gray, H. B. *Inorg. Chem.* **1962**, *1*, 111.

order of singlet−singlet excitations (^1E ($d_{xy} \rightarrow d_{xz},d_{yz}$) and $^1A_2$ ($d_{xy} \rightarrow d_{x^2-y^2}$)) is consistent with the assignments of ref 2. In ref 2 polarized single crystal data were obtained for a closely related complex, but the observed polarizations were not in accord with the expectations from group theory for C_{4v} symmetry. It should also be noted that all calculations predict the $^1A_1 \rightarrow {}^1A_2$ ($d_{xy} \rightarrow d_{x^2-y^2}$) to be at least an order of magnitude less intense than $^1A_1 \rightarrow {}^1E$ ($d_{xy} \rightarrow d_{xz},d_{yz}$), whereas experimentally the difference in intensities is not more than a factor of 2. Thus, some intensity borrowing mechanism, as put forward in ref 2, may indeed explain the unusual polarization pattern observed in the single-crystal experiments.

In summary, the calculations predict excited states at energies that compare well with the experimental data. The assignments of the first observed band at 11 800 cm^{-1} to a singlet−triplet transition appears to be unambiguous. Bands II and III can also safely be assigned to the ligand field transitions $^1A_1 \rightarrow {}^1E$ ($d_{xy} \rightarrow d_{xz},d_{yz}$) and $^1A_1 \rightarrow {}^1A_2$ ($d_{xy} \rightarrow d_{x^2-y^2}$). However, their precise order could not be unambiguously determined from comparison of calculation and experiment. Both INDO/S and TD-DFT calculations are potentially useful for the interpretation of the optical properties of these systems. Assuming that the assignments in ref 2 are correct, as is also supported by the calculated transition intensities, the TD-DFT calculations give better results for the d−d excitations but have the drawback that they predict a series of carboxylate-to-manganese LMCT transitions for **3** and **4** at unrealistically low energies, which is not consistent with the experimental observations. The INDO/S calculations on the other hand give more realistic values for these transitions but may get the order of the ^1E ($d_{xy} \rightarrow d_{xz},d_{yz}$) and $^1A_2$ ($d_{xy} \rightarrow d_{x^2-y^2}$) d−d excited states wrong. In any case, the considerably better agreement of the calculations with experiment for the structure **4**, with experimentally adjusted bond lengths, compared to **3** is noticeable and points to the necessity of having as accurate as possible structures available for accurate spectral predictions.

Comparison to Ligand Field Theory. Finally, we wish to discuss the validity of the ligand field model and the source of discrepancy between the INDO/S and the TD-DFT calculations. In TD-DFT, the major contributor to the transition energy from the occupied orbital *i* to the empty orbital *a* is simply the orbital energy difference $\Delta\epsilon_{ai} = \epsilon_a - \epsilon_i$, where ϵ is the orbital energy. The ground-state MO diagram is therefore a good indicator of the excitation spectrum in DFT, and it is not surprising that the TD-DFT calculation gives the $^1A_2$ ($d_{xy} \rightarrow d_{x^2-y^2}$) state *above* the ^1E ($d_{xy} \rightarrow d_{xz},d_{yz}$) state because the $d_{x^2-y^2}$ orbital is higher in energy than the d_{xz},d_{yz} orbitals.

This situation is different in Hartree−Fock based theories, where the singlet to singlet transition energy in zero order is given by

$$E(i \rightarrow a) = \Delta\epsilon_{ai} - J_{ia} + 2K_{ia}$$

Here J_{ia} is the Coulomb integral between two electrons in the molecular orbitals *i* and *a* and K_{ia} is the corresponding exchange integral. Values for the relevant integrals between the $1b_2$ (d_{xy}) and the four unoccupied manganese 3d-based orbitals and the zero order transition energies predicted from these values obtained from INDO/S calculations are listed in Table 8. It is evident that the exchange terms give a minor correction to the transition energies and that the majority of the effect is contained in the value of $\Delta\epsilon_{ai} - J_{ia}$, both parts of which are large. Importantly, the order of predicted transition energies does *not* follow the order of orbital energies. In fact, the INDO/S calculations predict the same ordering of orbitals as the DFT calculations. This effect is due to the considerably different values of the Coulomb integrals $J_{xy,x2-y2}$ and $J_{xy,xz/yz}$ that differ by more than 1 eV in the molecular orbital calculation (Table 8) where ligand field theory would predict them to be equal. This difference is due to the considerably different spatial characteristics of these orbitals (Figure 5). The 1e (d_{xz},d_{yz}) orbitals are fairly delocalized between the manganese and the nitrido ligand while $1b_1$ ($d_{x^2-y^2}$) is mostly localized on the manganese (Table 6, Figure 5). Since the repulsion of two electrons that are localized in similar regions of space is larger than the repulsion of electrons localized in different regions, it is conceivable that $J_{xy,x2-y2}$ is larger than $J_{xy,xz/yz}$ and consequently that the order of excited states may be reversed compared to the expectations from the one-electron orbital scheme. However, based on the discussion in the previous section, it is possible that the INDO/S method overestimates this difference somewhat, which would lead to an assignment that is reversed from the experimental one.

Table 8. Values for Coulomb and Exchange Integrals between the Metal Based Orbitals of **4** and Predicted Zero Order Transition Energies

orbitals	$\Delta\epsilon$ (eV)	J (eV)	$+2K$ (eV)	ΔE (eV)	ΔE (cm^{-1})
$^1b_2(d_{xy}) \rightarrow {}^1e(d_{xz})$	9.908	7.918	0.724	2.714	21 890
$^1b_2(d_{xy}) \rightarrow {}^1e(d_{yz})$	9.931	7.983	0.740	2.688	21 680
$^1b_2(d_{xy}) \rightarrow {}^1e(d_{x^2-y^2})$	10.742	9.250	0.552	2.044	16 480
$^1b_2(d_{xy}) \rightarrow {}^1e(d_{z^2})$	11.326	7.626	0.796	4.496	36 260

However, it should be realized that the anisotropic electron repulsion is a characteristic feature of high-valent metal complexes with strongly anisotropic covalency. It is this feature that makes ligand field theory a less reliable guide to the electronic structure and spectroscopy of these systems. In ligand field theory the treatment of electronic repulsion assumes metal orbitals with identical radial parts, and all anisotropy is, somewhat artificially, included in the one-electron part of the ligand field. Molecular orbital theory on the other hand correctly takes into account the actual bonding situation and acknowledges that the bonds formed between the high-valent metal ion and soft, strongly electron donating ligands are much more covalent than those formed with more normal, innocent ligands.

Acknowledgment. C.A.G. thanks the Alexander von Humboldt Foundation for a postdoctoral fellowship. F.N. gratefully acknowledges a Habilitationsstipendium from the Deutsche Forschungsgemeinschaft.

Supporting Information Available: Tables of crystallographic and structural refinement data, atom coordinates and U_{eq} values, bond lengths and angles, anisotropic thermal parameters, and calculated and refined positional parameters of hydrogen atoms for complexes **1** and **2** and figures of noncrystallographic data including ^1H and ^{13}C NMR spectra of **2** and a partial packing diagram of **1**. This material is available free of charge via the Internet at http://pubs.acs.org.

IC001370R